SP
RE

An Improved Power Conditioning System Based on Capacitor Current Feedback Active Damping of an LCL-Type Grid-Tied NPC Inverter

Majid Hosseinpour [1*], Mohammad Mohsen Rahimian [1], Navid Rasekh [1]

[1] Department of Electrical Engineering, University of Mohaghegh Ardabili, Ardabil, Iran.

Abstract

As grid-connected Photovoltaic (PV) based inverters are being used more, these systems play a more important role in the electricity generation by distributed power generators. Power injection to the grid needs to meet predefined standards. In order to meet the harmonics requirement of standards, they need an output filter. The connection through an LCL filter offers certain advantages, but it also brings the disadvantage of having a resonance frequency. LCL filter can easily help the system to satisfy these requirements but also introduce a resonance peak which makes the system control a challenging task. In this paper, a three-level Neutral Point Clamped (NPC) inverter is connected to the grid through an LCL filter. The injected current of the inverter is controlled using Proportional-Resonant (PR) controllers. The resonant peak of the filter is also damped using capacitor current feedback. A systematic mathematical design procedure for controller and filter capacitor current feedback coefficients is investigated in details. Simulations are carried out in MATLAB/Simulink environment and results depict suitable performance of the system with designed parameters

1. INTRODUCTION

Due to negative environmental impacts of fossil fuels,beside their limited resources, more attentions have been paid to renewable energy resources during recent years. As an example, Germany has planned to supply 100% of its electricity from renewable energy sources by 2050 [1,2]. However, renewable energy sources normally are in the form of Distributed Generation Units (DGUs) [3,4]. These DGUs not only benefit from the advantages of renewable energy sources, but also eliminate drawbacks of centralized energy production like transmission losses and development related issues.

*Corresponding Authors Email: hoseinpour.majid@uma.ac.ir

Photovoltaic (PV) systems are the most popular technologies used in DGUs. These systems benefit from flexibility of power electronic converters to extract maximum power from the solar radiation and deliver it to the grid/consumer.

Among different converter topologies [5-9], Neutral Point Clamped (NPC) inverter [10] is the most suitable choice for high and medium powers in medium voltage range. Although this converter generates a five level line to line voltage, to meet harmonic requirements of typically used standards e.g. IEEE std 1547 [11], an output filter is needed.

Many filter configurations have been introduced in literature [12-15]. Among them, LCL filter has superior performance in comparison with L and LC filters in high frequencies and also is not as complicated as high order filters [16,17]. However, the resonance peak of this filter can cause instability and thus should be damped.

Damping solutions can be generally classified as passive and active methods. Although passive methods can be simply implemented, e.g. by insertion of a parallel or series resistance with filter capacitor, they degrade filter performance and introduce extra power losses.

Active damping methods use control approaches to achieve the same goal. One of the most popular active damping methods is using the capacitor current feedback which results in suitable stability characteristic [18].

The main aim of DGUs is to provide suitable power quality to the grid, so choosing appropriate controller to control injected current to the grid is of high importance to deal with resonance frequency caused by LCL filter. Conventionally, Proportional-Integral (PI) controllers are the first choices to use in grid-connected systems. But as the order of the system using LCL filter increases, these controllers are unable to compensate for the system poles. Proportional Integral (PR) controller can tackle this issue by their higher order and help the system to track sinusoidal waveform reference with zero steady state error. Design and tuning of PR controller are issues that designers may face while applying LCL filter with such controller [19-20]. In [21] design of PR controller using direct pole placement has been discussed. In [22] PR controller design is based on desired transient performance. None of these works consist active damping. Recently, active damping design using current estimator has been proposed in [23] while it lacks a systematic method for tuning the PR controller. A grid-tied inverter with LCL filter using PI controller as the injected current regulator and considering active damping of filter capacitor current has been proposed in [24]. The latter work procedure is a step-by-step parameter design. A systematic method considering active damping and PR controller has been proposed in [25] to design control parameters while some presumptions of mentioned paper are not clear.

In this paper, a step by step design procedure is presented to design PR controllers' parameters as well as filter capacitor current feedback coefficient. The rest of this paper is organized as follows. Section II gives the system description and modelling. A mathematical step by step design procedure for the controllers and capacitor current feedback parameters is presented in section III. Simulation results

which depict suitable performance of the system are given in section IV. Finally, section V concludes this paper.

2. SYSTEM DESCRIPTION AND MODELLING

Per phase diagram of the system is illustrated in Fig. 1. As can be seen a NPC inverter is connected to the Point of Common Coupling (PCC) through an LCL filter. In this inverter every switch should block only half of the dc voltage which results in power rating of NPC inverter increasing two times greater than traditional two-level inverter, in case of using same switches. Furthermore, it's three-level output can help to reduce the filter size. A challenging task related to this inverter is balancing of input capacitors' voltages. In this paper a space vector modulation method proposed in [26] is used to deal with this issue.

Writing Kirchhoff's laws for the system results in (1):

$$\begin{cases} L_1 \dfrac{di_1}{dt} + R_1 i_1 = u_i - u_c - R_c i_c \\ L_2 \dfrac{di_g}{dt} + R_2 i_g = u_c - u_g - R_c i_c \\ C \dfrac{du_c}{dt} = i_c \\ i_1 = i_g + i_c \end{cases} \quad (1)$$

where, R_2 and R_c are equivalent series resistances of filter inductances and capacitor. However, as they are neglected through design procedure, they are not shown in Fig. 1. The equivalent block diagram of the system is shown in Fig. 2. As can be seen, the actual injected current to the grid is differentiated from the reference current,

which is calculated by the upstream power control. The error goes through a PR controller to create reference voltages for the inverter.

To compensate filter resonance peak, a feedback of filter capacitor current is added to these references. Design of controller parameters and capacitor current feedback coefficient is discussed in the following section.

3. DESIGN PROCEDURE

3.1. Control Scheme Modelling

The diagram shown in Fig. 2 can be simplified to the one in Fig. 3 in which $G_1(s)$, $G_2(s)$ and $G_{PR}(s)$ a:

$$G_1(s) = \frac{K_{inv} G_{PR}(s)}{CL_1 s^2 + K_{inv} K_{AD} Cs + 1} \quad (2)$$

$$G_2(s) = \frac{CL_1 s^2 + K_{inv} K_{AD} Cs + 1}{L_1 L_2 Cs^3 + L_2 CK_{AD} K_{inv} s^2 + (L_1 + L_2)s} \quad (3)$$

$$G_{PR}(s) = K_P + \frac{2 K_r \omega_{PRc} s}{s^2 + 2\omega_{PRc} s + \omega_1^2} \quad (4)$$

K_{AD} is the active damping factor and $G_{PR}(s)$ is PR controller transfer function. According to Fig. 3, the open loop transfer function is calculated as following:

$$T(s) = \frac{K_{gi} K_{AD} G_{PR}(s)}{L_1 L_2 Cs^3 + L_2 CK_{AD} K_{inv} s^2 + (L_1 + L_2)s} \quad (5)$$

If the grid current be considered as the effects of reference current and grid voltage, it can be inferred that:
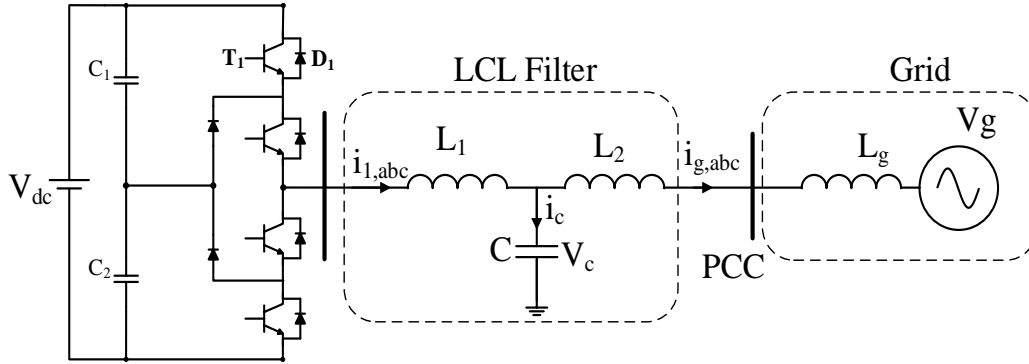
Fig. 1. Per phase diagram of the system.
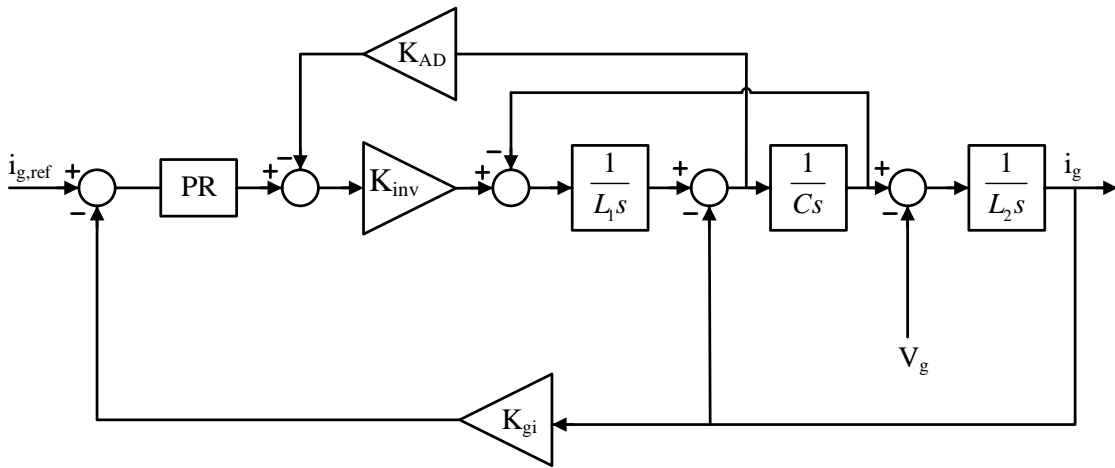
Fig. 2. System control diagram.

$$i_g(s) = i_{g1}(s) + i_{g2}(s) \qquad (6)$$

where

$$\begin{cases} i_{g1}(s) = \dfrac{1}{K_{gi}} \dfrac{T(s)}{1+T(s)} i_{ref}(s) \\[4mm] i_{g2}(s) = -\dfrac{G_2(s)}{1+T(s)} V_g(s) \end{cases} \qquad (7)$$

According to Fig. 4 and considering φ as the angle between $i_{g1}(s)$ and $i_g(s)$:

$$\begin{aligned} \tan(\varphi) &= \left| \frac{i_{g2}(s)}{i_{g1}(s)} \right| \\[3mm] &= \left| \frac{K_{gi} G_2(s) V_g(s)}{T(s) i_{ref}(s)} \right|_{s=j\omega_1} \\[3mm] &= \left| \frac{K_{gi} G_2(j\omega_1)}{T(j\omega_1)} \frac{V_g(j\omega_1)}{i_{ref}(j\omega_1)} \right| \end{aligned} \qquad (8)$$

By substituting $s = j\omega_1$ in $G_{PR}(s)$:

$$G_{PR}(j\omega_1) = K_P + \frac{2K_r\omega_{PRc}j\omega_1}{(j\omega_1)^2 + 2\omega_{PRc}j\omega_1 + \omega_1^2} \quad (9)$$
$$= K_P + K_r$$

The capacitor of LCL filter can be ignored since the LCL filter resonance frequency is much greater than the fundamental frequency [25]:

$$\begin{cases} C = 0 \\ G_2(j\omega_1) = \dfrac{1}{(L_1 + L_2)(j\omega_1)} \end{cases} \quad (10)$$

Thus, it can be deduced that:

$$\begin{cases} \tan(\varphi) = \left|\dfrac{K_{gi}}{T(j\omega_1)(L_1 + L_2)(j\omega_1)}\right|\left|\dfrac{V_g(j\omega_1)}{i_{ref}(j\omega_1)}\right| \\ T(j\omega_1) = \dfrac{K_{gi}}{\tan(\varphi)(L_1 + L_2)(\omega_1)} \cdot \dfrac{V_g}{I_{ref}} \end{cases} \quad (11)$$
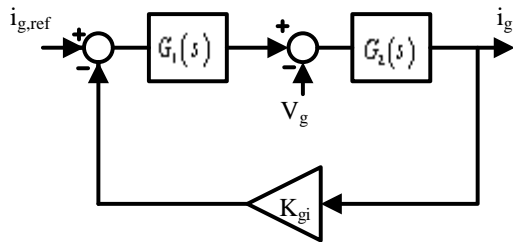
Fig. 3. Equivalent control diagram of injected current.
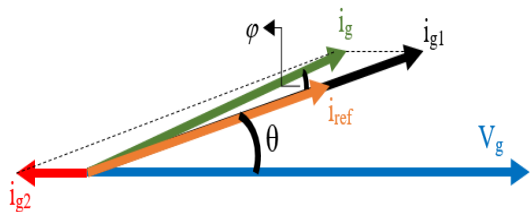
Fig. 4. Phasor diagram of the grid voltage and injected grid current.

V_g is the root mean square (RMS) value of the grid voltage and I_{ref} is the RMS value of the reference current. T_{f1} is considered as the magnitude of the open loop transfer function at f_1 (fundamental frequency), in dB.

$$\begin{aligned} T_{f1} &= 20\log|T(j\omega_1)| \\ &= 20\log(\frac{K_{gi}V_g}{\tan(\varphi)I_{ref}(L_1 + L_2)(\omega_1)}) \end{aligned} \quad (12)$$

According to Fig. 4 current error E_A can be calculated as following:

$$\begin{aligned} E_A &= \frac{|K_{gi}i_g(j\omega_1)| - I_{ref}}{I_{ref}} \\ &= \frac{K_{gi}|i_{g1}(j\omega_1)/\cos\varphi|}{I_{ref}} - 1 \end{aligned} \quad (13)$$

Substituting $i_{g1}(s)$ from (7) to (12), E_A can be expressed as:

$$E_A = \left|\frac{T(j\omega_1)}{1 + T(j\omega_1)}\right|\frac{1}{\cos\varphi} - 1 \quad (14)$$

If $T_{f1} \geq 40$ dB then $1 + T(j\omega_1) \approx T(j\omega_1)$, so (14) can be rewritten:

$$E_A = \left|\frac{T(j\omega_1)}{1 + T(j\omega_1)}\right|\frac{1}{\cos\varphi} - 1 \approx \frac{1}{\cos\varphi} - 1 \quad (15)$$

According to (15) and Fig. 4, to achieve zero error, the $\cos\varphi = 1$, which means $\varphi = 0°$ As the phase of the reference current is defined by a phase locked loop (PLL) of the grid voltage, $i_{ref}(s)$ and $V_g(s)$ have the same phase ($\theta = 0°$).

3.2. Proportional–Resonant Controller

3.2.1. Proportional Gain (k$_P$)

The resonance frequency of LCL filter can be obtained by equation (9).

$$f_{res} = \frac{1}{2\pi}\sqrt{\frac{L_1 + L_2}{L_1 L_2 C}} \qquad (16)$$

The crossover frequency (f_c) value is usually chosen lower than switching frequency (f_{sw}) to prevent the effect of attenuating high frequency noise. Resonance frequency of the LCL filter is typically constrained in the range of $f_{sw}/4$ to $f_{sw}/2$ in order to suppress harmonics and function with good dynamics. To fulfil appropriate design and suitable performance of the grid-connected LCL NPC inverter, f_c is chosen a value close to $f_{sw}/10$. Since f_c is about nearly ten times smaller than f_{sw} and also is smaller than resonance frequency of LCL filter, the impact of the capacitor can be overlooked [25][27], so the open loop transfer function of the system can be derived as:

$$\left|T(s)\right| \approx \left|\frac{K_{gi}K_{inv}G_{PR}(s)}{(L_1 + L_2)s}\right| \qquad (17)$$

PR controller equation can be simplified since the cut-off frequency is greater than the fundamental frequency, therefore, the resonance term of PR controller is ignored and also (18) is concluded.

$$G_{PR}(j\omega_c) = K_P + K_r \approx K_P \qquad (18)$$

The open loop transfer function can be rewritten as follows:

$$\left|T(j\omega_c)\right| \approx \left|\frac{K_{gi}K_{inv}K_P}{(L_1 + L_2)j\omega_c}\right| \qquad (19)$$

The amplitude of system frequency response is zero in cut-off frequency and it can be used to calculate proportional gain.

$$20\log\left|G(j2\pi f_c)\right| \approx$$
$$20\log\left|\frac{K_{gi}K_{inv}K_P}{(L_1 + L_2)j\omega_c}\right| = 0 \qquad (20)$$

$$K_P = \frac{2\pi f_c(L_1 + L_2)}{K_{gi}K_{inv}} \qquad (21)$$

3.2.2. Resonant Gain (K_r)

Considering PR controller transfer function as (4), in cut off frequency ($f = f_1$) (4) can be rewritten as :

$$\begin{aligned} G_{PR}(j\omega_1) &= K_P \\ &+ \frac{2K_r\omega_{PRc}(j\omega_1)}{(j\omega_1)^2 + 2\omega_{PRc}(j\omega_1) + \omega_1^2} \\ &= K_P + K_r \end{aligned} \qquad (22)$$

According to (17) and (21), it is inferred that:

$$\left|T(s)\right|_{s=j\omega_1} \approx \left|\frac{K_{gi}K_{inv}(K_P + K_r)}{(L_1 + L_2)(j\omega_1)}\right| \qquad (23)$$

Considering (12) leads to (24) and (25)

$$\begin{cases} T_{f1} = 20\log\left|T(j\omega_1)\right| \\ T_{f1} = 20\log\left|\dfrac{K_{gi}K_{inv}(K_P + K_r)}{(L_1 + L_2)(j\omega_1)}\right| \end{cases} \qquad (24)$$

$$K_r = \frac{2\pi(L_1 + L_2)}{K_{gi}K_{inv}}(10^{\frac{T_{f1}}{20}}f_1 - f_c) \qquad (25)$$

By substituting $j\omega_c$ for s in (4):

$$G_{PR}(j\omega_c) = K_P + \frac{2K_r\omega_{PRc}(j\omega_c)}{(j\omega_c)^2 + 2\omega_{PRc}(j\omega_c) + \omega_1^2} \qquad (26)$$

As $(j\omega_c)^2 + 2\omega_{PRc}(j\omega_c)$ is far greater than ω_1^2, so the term ω_1^2 can be ignored and $G_{PR}(s)$ will be:

$$K_r = \frac{\left(\frac{L_1 + L_2}{L_2 C}\right) - 2\pi L_1 f_c^2 - K_{AD}K_{inv}f_c \tan(PM)}{K_{AD}K_{inv}f_c + \left(\left(\frac{L_1 + L_2}{L_2 C}\right) - 2\pi L_1 f_c^2\right)\tan(PM)} \cdot \frac{\pi f_c K_P}{w_{PRc}} \qquad (29)$$

3.3. Capacitor Current Feedback Coefficient (K_{AD})

By substituting (21) and (24) in (29), K_{AD} is calculated as:

$$K_{AD} = \frac{(L_1 + L_2)/L_2 C - 2\pi L_1 f_c^2}{K_{inv}f_c}$$

$$\times \frac{\pi f_c^2 - (10^{\frac{T_{f1}}{20}}f_1 - f_c)w_{PRc}\tan(PM)}{(10^{\frac{T_{f1}}{20}}f_1 - f_c)w_{PRc} + \pi f_c^2 \tan(PM)} \qquad (30)$$

The gain margin (GM) of the system at resonance frequency is calculated as following:

$$GM = -20\log|T(j\omega_r)| \qquad (31)$$

$$G_{PR}(s) = K_P + \frac{2K_r\omega_{PRc}}{s} \qquad (27)$$

Assuming desired phase margin for the system to be PM, it can be inferred that:

$$\pi + \angle T(j\omega_c) = PM \qquad (28)$$

Using (5) together with (27) and (28), K_r can be expressed as:

Substituting $s = j\omega_r$ into (4) it's inferred that:

$$|G_{PR}(j\omega_r)| = \left|K_P + \frac{2K_r\omega_{PRc}(j\omega_r)}{(j\omega_r)^2 + 2\omega_{PRc}(j\omega_r) + \omega_1^2}\right| \qquad (32)$$

As the denominator of the term, which contains K_r, is far greater than the numerator part, this part can be ignored and (30) can be rewritten:

$$|G_{PR}(j\omega_r)| = K_P \qquad (33)$$

Substituting (21) and (32) into (5) considering $s = j\omega_r$, $T(j\omega_r)$ will be:

$$T(j\omega_r) = A/B = \frac{2\pi f_c(L_1 + L_2)}{-(\omega_r)^2(L_2 C K_{AD}K_{inv}) - j\omega_r(L_1 L_2 C\omega_r^2 + (L_1 + L_2))} \qquad (34)$$

$$\begin{cases} |A| = 2\pi f_c \left(L_1 + L_2 \right) \\ |B| = \dfrac{L_1 + L_2}{L_1} \sqrt{(K_{AD}K_{inv})^2 + 4\omega_r^{\ 2}L_1^{\ 2}} \end{cases} \quad (35)$$

As $(K_{AD}K_{inv})^2$ is far greater than $4\omega_r^{\ 2}L_1^{\ 2}$ the latter term can be ignored, so $T(j\omega_r)$ can be simplified to (36).

$$|T(j\omega_r)| = \frac{|A|}{|B|} = \frac{2\pi f_c L_1}{K_{AD}K_{inv}} \quad (36)$$

Considering (31) and (36), the minimum value of K_{AD} is expressed by (37):

$$K_{AD} = 10^{\frac{GM}{20}} \cdot \frac{2\pi f_c L_1}{K_{inv}} \quad (37)$$

3.4. Design Considerations

The magnitude of the open loop transfer function at fundamental frequency, T_{f1}, is the starting point for controller parameter design. As mentioned in (15), T_{f1} should be greater than 40 dB. In this paper T_{f1} is supposed to be 45 dB.

After calculating K_P and defining T_{f1}, the next step is to calculate minimum resonant gain K_r by equation (24). Then, the upper boundary of K_{AD} is obtained using (30). The lower boundary of K_{AD} depends on GM and cut-off frequency rather than intrinsic parameters of the system. By applying (36) and supposing the $GM = 5\ dB$ at resonance frequency, the minimum value of K_{AD} is obtained. After all, when the range of K_{AD} is defined, and the suitable value of K_{AD} is chosen, the upper boundary of K_r is calculated using (29). It should be noted that by decreasing the value of K_{AD}, the phase

margin of the openloop system increases. To choose a suitable value for K_r, it should be taken into account that greater K_r leads to smaller GM.

4. SIMULATION

In this section, the system with the parameters designed using described method in section III has been simulated in MATLAB/Simulink environment. A 200 kVA NPC inverter is chosen and it's parameters are adopted from [28] and given in Table 1. According to LCL filter parameters, resonance frequency of LCL filter is 5890 Hz and cut-off frequency is chosen 1475 Hz. Using (21), K_P becomes 0.1237. By employing (24) the lower boundary of 0.6921 is calculated for K_r. The upper boundary for the active damping coefficient using (30) is obtained as 0.0169. Equation (37) gives the lower boundary of 0.00237 for K_{AD}. K_{AD} is chosen 0.0003 to achieve sufficient phase margin for the system. After definition of K_{AD}, the upper limit of K_r is calculated using the defined value of K_{AD} and (29), so K_r is in the range of 0.6921 to 42.38. Considering suitable phase margin and gain margin, K_r is set to be 5.

To analyze the credibility of the proposed tuning of the control parameters, the control system is supposed to be in a weak grid, where the grid impedance is considerably inductive. So (L_g) is increased from L_g=100µH to L_g=3100µH to model a very weak grid, with steps of 200 µH. As shown in Fig. 5, by increasing the grid side inductance, the closed loop poles of the

control system don't exceed the unit circle in the z-plane and the system performs well maintaining the system's stability.

To achieve a better understanding of the control system performance during a highly inductive grid (L_g=3100µH), root locus analysis of such system is done by MATLAB. As depicted in Fig. 6, the system root loci are fully placed in Left Half Plane (LHP) and it's stable even in a very inductive grid. The zeros of the closed loop system in Fig. 5 which are located on the boundary of the unit circle, represent those pair of zeros on the imaginary axis in Fig. 6. By scrutinizing the root locus analysis in different forms of the weak grid (L_g=100µH to L_g=3100µH), in the vicinity of S=-75, a zero and a pole are always present for any Lg values and this zero will eliminate the impact of the corresponding pole. The system would be stable even if this corresponding pole is a dominant one since there is a sufficient distance from imaginary axis and the system expresses a good dynamic behavior.

Fig. 7 shows bode diagram of the open-loop system. As can be seen with designed parameters, a phase margin of 76.1 degrees and gain margin of 6.91 dB are achieved.

A comparison between the system with and without active damping scheme is illustrated in Fig. 8. Sharp rise of frequency response magnitude due to LCL filter resonance can be seen around resonance frequency. As it is shown, this sharp rise is completely softened using active damping.

Injected active and reactive powers to the grid are shown in Fig. 9. At 0.2 sec, the active power reference decreases by 50 percent and back to its previous value at 0.25. Reactive power reference is always held at zero.

Table 1. *Parameters.*

Parameter	Value
Inverter side inductor (L_1)	100 µH
Grid side inductor (L_2)	270 µH
LCL filter capacitor (C)	10 µF
Fundamental frequency (f_1)	50 Hz
Switching frequency (f_{sw})	10 kHz
DC link voltage (V_{dc})	1200 v
Grid phase voltage (RMS)	480 v
Grid current feedback Coefficient (K_{gi})	0.04
Controller Cut off frequency (ω_{PRc})	10 rad
K_{inv}	692 v
Cut off Frequency f_c	1475 Hz
Phase Margin (PM)	45˚
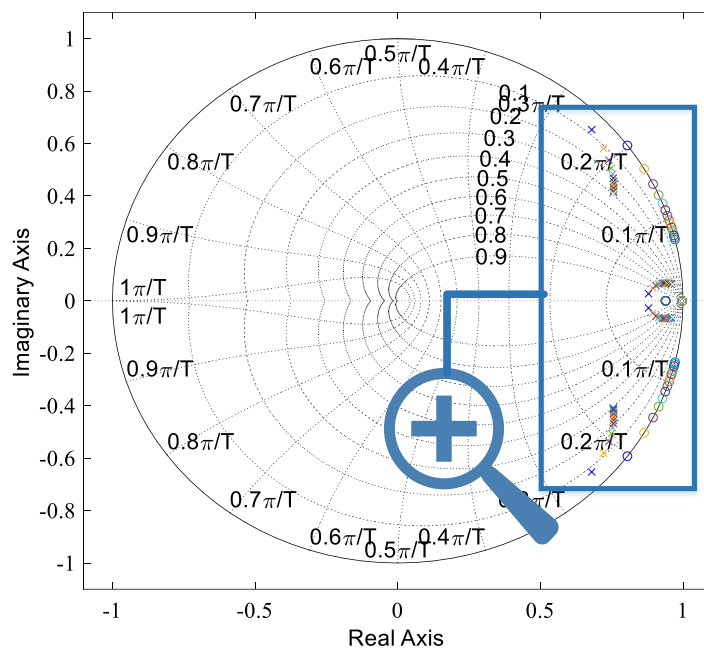
(a)
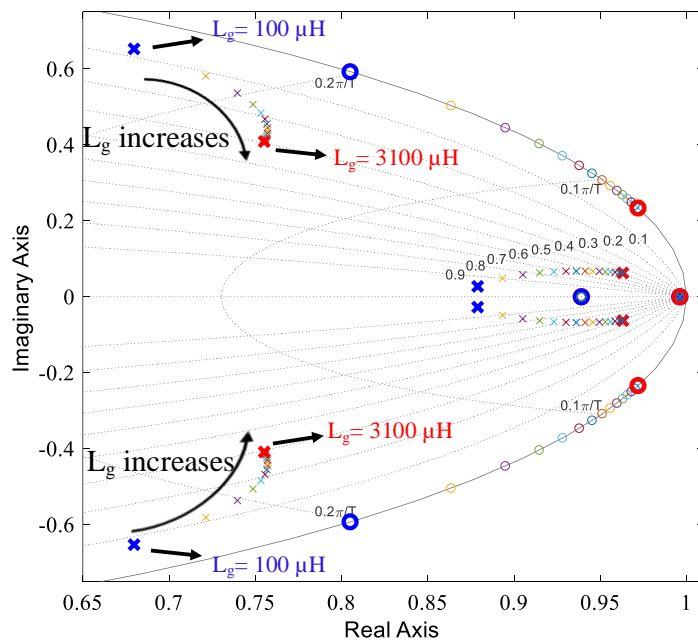
(b)

Fig. 5. (a) Pole-Zero map of the system by varying L$_g$, (b) the magnified part of the pole-zero map.

As can be seen, delivered powers to the grid follow their references. Grid currents are also presented in Fig. 10, where their changes, due to reference power changes, can be clearly seen. From these figures, it can be deduced that the PR controllers, with designed parameters, have suitable performance.
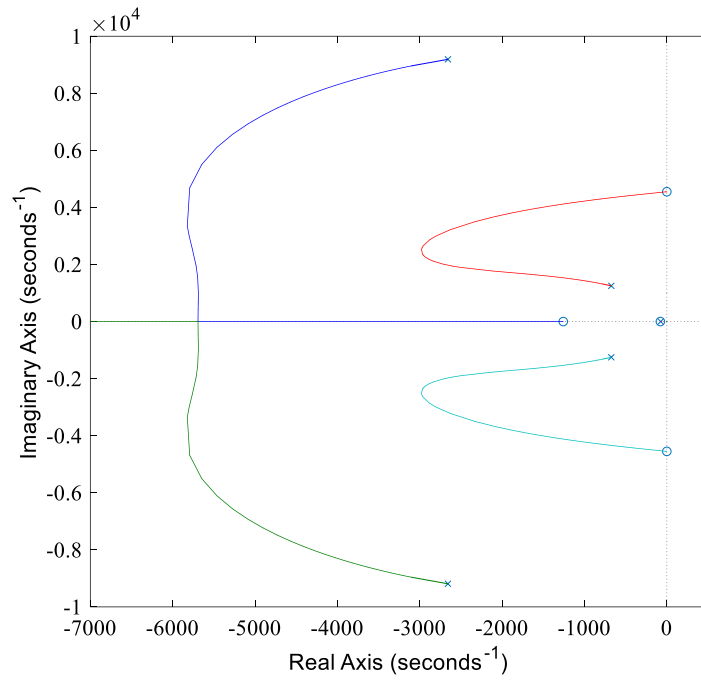
Fig. 6. Root loci of the closed loop control system in a highly inductive grid L_g=3100μH.
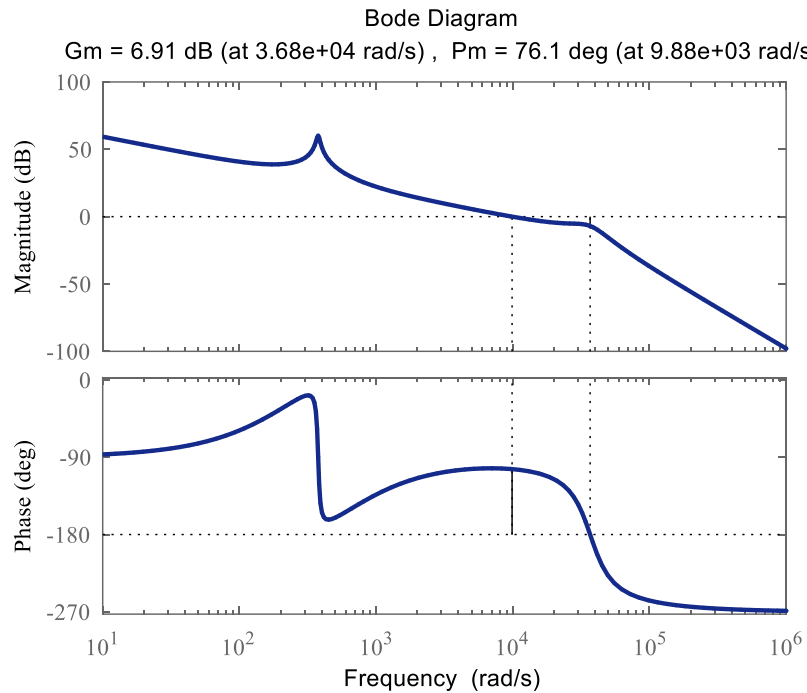
Fig. 7. Open loop bode diagram of the system ($K_{AD} = 0.003$ and $K_r = 5$)

.
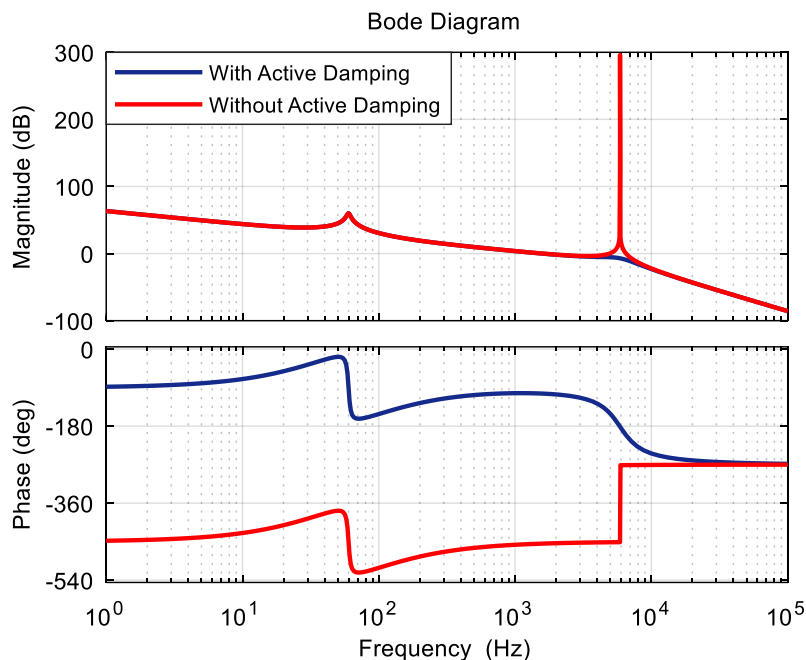
Fig. 8. Bode diagram of the open loop system with and without active damping.
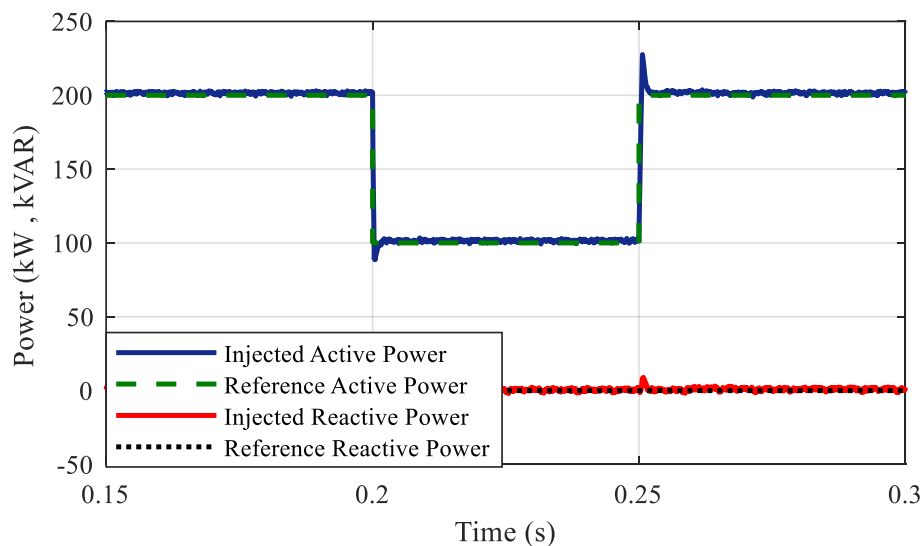
Fig. 9. Active and Reactive power delivered to the grid.

Harmonic spectra of injected current to the grid is shown in Fig. 11. As can be seen, Total Harmonic distortion (THD) of the injected current is far below 5% which shows the effectiveness of using LCL filter to follow restrictions of IEEE std 1547 [11].

Fig. 12 shows grid phase voltage and current in case a voltage sag of 0.1 p.u. occurs during t=0.1 second to t=0.2 second. Another case, in which a 0.1 p.u. voltage swell happens in t=0.1 second to t=0.2 second, is depicted in Fig. 13. Simulation results of grid voltage fluctuations, causing inductance

value variation, verify that the system with proportional resonant control with calculated parameters maintains its stability in both cases.
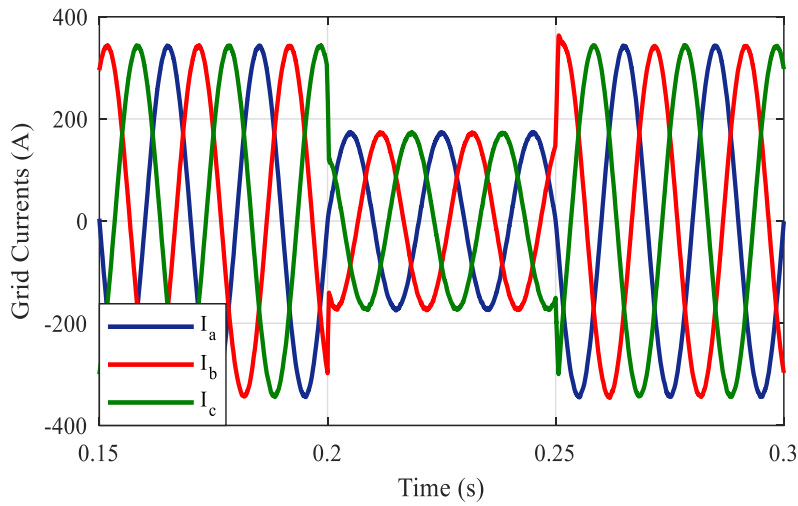
Fig. 10. Injected currents to the grid.
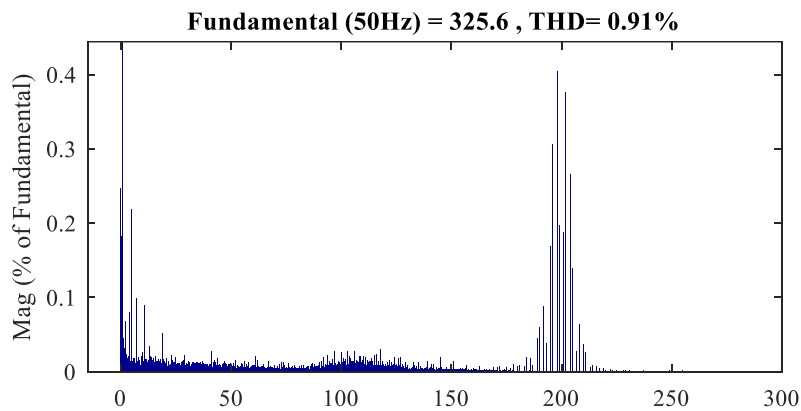
Fig. 11. Harmonic spectra of injected current to the grid.
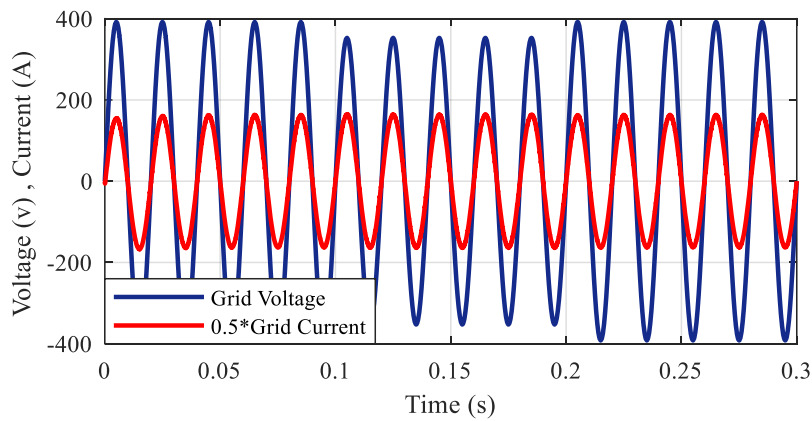
Fig. 12. Grid phase voltage and injected current during grid voltage sag in which L_2 is increased by 10%.
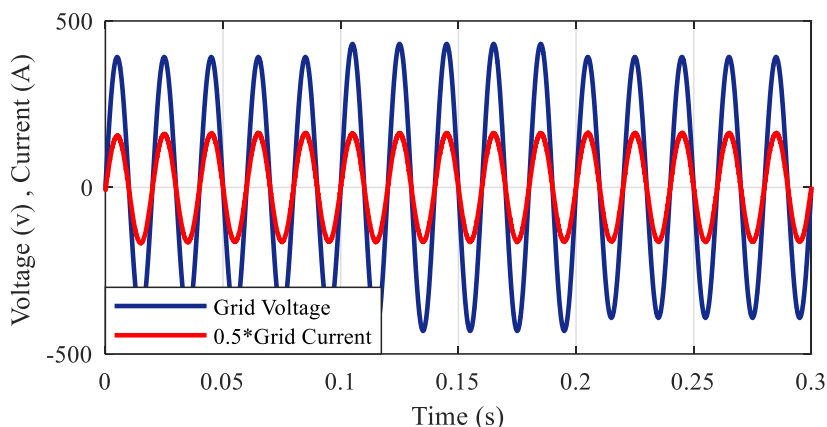
Fig. 13. Grid phase voltage and injected current during grid voltage swell in which L$_2$ is decreased by 30%.

As DGUs may be exposed to weak grid, it's important for the system to maintain its stability during grid voltage fluctuations. In a situation in which an inverter is connected to a weak grid, the grid impedance is inductive. Hence, the grid inductance variation can be modelled as variation in grid side inductance (L$_2$).

5. CONCLUSION

Controlling of a grid-connected LCL inverter, due to resonance peak of the filter, is a challenging task. In this paper, a systematic design procedure based on mathematical analysis of the system model for PR controller and capacitor current feedback active damping parameters is presented. The system stability using designed parameters is investigated. Moreover, to examine the robustness of the system, grid voltage and inductance are varied. Simulation results depict suitable performance of the system during these variations. Although NPC inverter is used in this paper, the presented method can be applied to any other single or three phase system.

REFERENCES

[1] G. A. C. on the Environment, "Pathways towards a 100% renewable electricity system," 2011.

[2] M.B. Sharifian, Y. Mohamadrezapour, M. Hosseinpour, S. Torabzade, Maximum power control of grid connected variable speed wind system through back to back converters. Journal of Applied sciences, Vol. 8, no. 23, pp.4416-4421, 2008.

[3] F. Blaabjerg, Y. Yang, D. Yang, and X. Wang, "Distributed Power-Generation Systems and Protection," Proc. IEEE, vol. 105, no. 7, pp. 1311–1331, 2017.

[4] M. Hosseinpour, M. Mohamadian, A.Y. Varjani, "RDFT based control of a 3-phase 4-leg shunt active power filter under unbalanced load and non-ideal mains voltage conditions," In 2014 22nd Iranian Conference on Electrical Engineering (ICEE), pp. 739-745, 2014.

[5] M. Hosseinpour, A. Seifi, A. Dejamkhooy, F. Sedaghati, "Switch count reduced structure for symmetric bi-directional multilevel inverter based on switch-diode-source cells," IET Power Electronics, Vol. 13, no. 8, pp. 1675-1686, 2020.

[6] S.H.L. Majareh, F. Sedaghati, M. Hosseinpour, S.R. Mousavi-Aghdam, "Design, analysis and implementation of a generalised topology for multilevel inverters with reduced circuit devices," IET Power Electronics, Vol. 12, no. 14, pp.3724-3731. 2019.

[7] S.G. Ardakani, M. Hosseinpour, M. Shahparasti, M. Siahi, "Direct torque control of low-voltage three-phase induction motor using a three-level eight-switch inverter," Arabian Journal for Science and Engineering, Vol. 44, no. 8, pp.7121-7131, 2019.

[8] M. M.Rahimian, M. Hoseinpour, A. Dejamkhooy. "A modified phase-shifted pulse width modulation to extend linear operation of hybrid modular multi-level converter." Journal of Operation and Automation in Power Engineering, Vol. 6, no. 2, pp. 183-192, 2018.

[9] M. Hosseinpour, S. Mansoori, H. Shayeghi, "Selective Harmonics Elimination Technique in Cascaded H-Bridge Multi-Level Inverters Using the Salp Swarm Optimization Algorithm," Journal of Operation and Automation in Power Engineering, Vol. 8, no. 1, pp.32-42, 2020.

[10] A. Poolad, M. Shahparasti, M. Hosseinpour, "Supplying Three Phase, Four Wire, Unbalanced and Non-Linear, Asymmetric Ohmic-Inductive Load by NPC Inverter Based on Method Predictive Control." Signal Processing and Renewable Energy, Vol. 3, no. 4, pp. 1-21, 2019.

[11] "IEEE Standard for Interconnecting Distributed Resources with Electric Power Systems," IEEE Std 1547-2003. pp. 1–28, 2003.

[12] N. Rasekh, M. Hosseinpour, "Adequate Tuning of LCL filter for Robust Performance of Converter Side Current Feedback Control of Grid Connected Modified–Y-Source Inverter," International Journal of Industrial Electronics, Control and Optimization, Vol. 3, no. 3, pp. 365-378, 2020.

[13] M. Hosseinpour, N. Rasekh, "A Single-Phase Grid-tied PV based Trans-Z-Source Inverter Utilizing LCL filter and Grid Side Current Active Damping," Journal of Energy Management and Technology, Vol. 3, no. 3, pp.67-77, 2019.

[14] N. Rasekh, M.M. Rahimian, M. Hosseinpour, A. Dejamkhooy, A. Akbarimajd, "A step by step design procedure of PR controller and capacitor current feedback active damping for a LCL-type grid-tied T-type inverter," In 2019 10th International Power Electronics, Drive Systems and Technologies Conference (PEDSTC), pp. 612-617. 2019.

[15] R. N. Beres, X. Wang, M. Liserre, F. Blaabjerg, and C. L. Bak, "A Review of Passive Power Filters for Three-Phase Grid-Connected Voltage-Source Converters," IEEE J. Emerg. Sel. Top.

Power Electron., vol. 4, no. 1, pp. 54–69, 2016.

[16] M. Huang, F. Blaabjerg, Y. Yang, and W. Wu, "Step by step design of a high order power filter for three-phase three-wire grid-connected inverter in renewable energy system," in 2013 4th IEEE International Symposium on Power Electronics for Distributed Generation Systems (PEDG), 2013, pp. 1–8.

[17] N. Rasekh, M. Hosseinpour, "LCL filter design and robust converter side current feedback control for grid-connected Proton Exchange Membrane Fuel Cell system," International Journal of Hydrogen Energy, Vol. 45, no. 23, pp. 13055-13067, 2020.

[18] M. Malinowski and S. Bernet, "A simple voltage sensorless active damping scheme for three-phase PWM converters with an LCL filter," IEEE Trans. Ind. Electron., vol. 55, no. 4, pp. 1876–1880, 2008.

[19] M. Hosseinpour and A. Dejamkhooy, "Control and power sharing among parallel three-phase three-wire and three-phase four-wire inverters in the presence of unbalanced and harmonic loads," IEEJ Trans. Electr. Electron. Eng., vol. 13, no. 7, pp. 1027–1033, 2018.

[20] M. Hosseinpour, M. Mohamadian, A.Y. Varjani, "Design and analysis of the droop-controlled parallel four-leg inverters to share unbalanced and nonlinear loads," Przegląd Elektrotechniczny, Vol. 90, no. 1, pp.105-110, 2014.

[21] B. Li, W. Yao, L. Hang, and L. M. Tolbert, "Robust proportional resonant regulator for grid-connected voltage source inverter (VSI) using direct pole placement design method," IET Power Electron., vol. 5, no. 8, pp. 1367–1373, 2012.

[22] A. Kuperman, "Proportional-Resonant Current Controllers Design Based on Desired Transient Performance," IEEE Trans. Power Electron., vol. 30, no. 10, pp. 5341–5345, 2015.

[23] R. A. Liston, E. G. Carati, R. Cardoso, J. P. da Costa, and C. M. de O. Stein, "A Robust Design of Active Damping With a Current Estimator for Single-Phase Grid-Tied Inverters," IEEE Trans. Ind. Appl., vol. 54, no. 5, pp. 4672–4681, 2018.

[24] C. Bao, X. Ruan, X. Wang, W. Li, D. Pan, and K. Weng, "Step-by-Step Controller Design for LCL-Type Grid-Connected Inverter with Capacitor–Current-Feedback Active-Damping," IEEE Trans. Power Electron., vol. 29, no. 3, pp. 1239–1253, 2014.

[25] N. Zhang, H. Tang, and C. Yao, "A Systematic Method for Designing a PR Controller and Active Damping of the LCL Filter for Single-Phase Grid-Connected PV Inverters," pp. 3934–3954, 2014.

[26] J. Pou, D. Boroyevich, and R. Pindado, "New feedforward space-vector PWM method to obtain balanced AC output voltages in a three-level neutral-point-clamped converter," IEEE Trans. Ind. Electron., vol. 49, no. 5, pp. 1026–1034, 2002.

[27] H. Akagi, "Active Harmonic Filters," Proc. IEEE, vol. 93, no. 12, pp. 2128–2141, 2005.

[28] Y. Jiao and F. C. Lee, "LCL filter design and inductor ripple analysis for 3-level NPC grid interface converter," in 2014 IEEE Energy Conversion Congress and Exposition (ECCE), 2014, pp. 1911–1918.